Origin of thermal fixing in photorefractive lithium niobate crystals

K. Buse,* S. Breer, K. Peithmann, S. Kapphan, M. Gao, and E. Krätzig
Universität Osnabrück, Fachbereich Physik, D-49069 Osnabrück, Germany
(Received 18 November 1996)

Macroscopic light patterns are thermally fixed in photorefractive iron- or copper-doped $LiNbO_3$ crystals with different hydrogen concentrations. Spatially resolved absorption measurements reveal unambiguously that migrating hydrogen ions compensate for the space-charge fields at enhanced temperatures if the hydrogen concentration is large enough. However, in crystals with small hydrogen concentrations thermal fixing is also possible and another compensation mechanism appears. Partial depolarization of the crystals does not contribute to the charge compensation processes. The refractive-index pattern is developed by homogeneous illumination and measured by an interferometric technique. The development process is described considering the spatially modulated concentrations of filled and empty electron traps, which cause spatially modulated currents, even for homogeneous illumination. [S0163-1829(97)06220-6]

I. INTRODUCTION

Electronic components have been replaced more often by optical devices because of the advantageous properties of light.[1] All optical communication networks with fiber optics and volume holographic memories are under development;[2] materials are required for the realization of these advanced devices. Photorefractive crystals offer many fascinating possibilities for applications in technical optics. The light-induced refractive-index changes enable, e.g., production of thick phase gratings with outstanding Bragg selectivities and large diffraction efficiencies.[3] These gratings are of special interest for wavelength stabilization of diode lasers or wavelength multiplexing and demultiplexing.

In photorefractive crystals, inhomogeneous illumination excites charge carriers from impurities into the conduction or valence band and these charge carriers move because of drift, diffusion, and the bulk photovoltaic effect.[4] Because the excitation rate in darker regions is smaller than in brighter regions, electric space-charge fields build-up and modulate the refractive index via the electro-optic effect, e.g., in the case of $LiNbO_3$:Fe it is known that electrons are excited from Fe^{2+} ions into the conduction band and trapped by Fe^{3+} ions.[5] A common problem of photorefractive devices is that homogeneous illumination erases the stored light pattern. Different methods for reading without erasure have been developed. Permanent refractive-index changes, which cannot be erased by light, are obtained by thermal[6,7] and electrical fixing,[8,9] while other techniques are based on recording with light of high photon energy and read-out with light of low photon energy.[10–15] Thermal fixing is of special interest too because this method enables the superposition of many holograms with high diffraction efficiencies.[16] Thermal fixing was discovered and intensively investigated in $LiNbO_3$, but is also possible in $LiTaO_3$,[17] $Bi_{12}SiO_{20}$ (BSO),[18] $KNbO_3$,[19,20] and $BaTiO_3$.[21,22]

A light pattern is ''thermally fixed'' by heating the crystal during or after illumination. At enhanced temperatures the electric space-charge field is compensated. After cooling the crystal to room-temperature homogeneous illumination ''develops'' the stored refractive-index pattern. A detailed understanding of these processes is required for tailoring of crystals for special applications.

In this investigation, we perform thermal fixing experiments of macroscopic Gaussian intensity patterns in iron- or copper-doped $LiNbO_3$ crystals and measure spatially resolved Fe^{2+}, Cu^{+}, and H^{+} concentrations and changes of refractive index. The results are compared with computer simulations. The aim is to reveal unambiguously the origin of the two main steps of thermal fixing: Compensation of the space-charge fields and development by homogeneous illumination.

II. REVIEW OF PREVIOUS WORK

A. Compensation of space-charge fields

Compensation of the space-charge fields at enhanced temperatures is crucial for thermal fixing. Migration of ions or of crystal defects, reorientation effects, or a partial depolarization of the crystals may compensate for the space-charge fields.[23–25] Several investigations were carried out to reveal the dominant compensation mechanism.

Staebler and Amodei measured the time constant of space-charge field compensation in the temperature range 80–300 °C and found that an Arrhenius law is fulfilled with a thermal activation energy of 1.1 eV.[26] From the time constants the corresponding conductivities were estimated, which are in excellent agreement with directly measured values. At temperatures around 1000 °C $LiNbO_3$ has an ionic conductivity,[27,28] and an extrapolation of the conductivity values of Staebler and Amodei to this temperature region shows fairly good agreement with literature values.[27,28] This leads to the conclusion that ionic conductivity is the major contribution to the fixing process. However, this conclusion is doubtful because of the much higher thermal activation energy 1.5–1.9 eV at 1000 °C.[27,28]

Smith *et al.* discovered that hydrogen is present in $LiNbO_3$; the OH^{-} stretching vibrations cause an absorption band at 2870 nm.[29] Bollmann and Stöhr showed that in the temperature range 400–1000 °C hydrogen is the origin of the conductivity with a thermal activation energy of 1.11 eV;[30] this agrees with the activation energy obtained from the ther-

mal fixing experiments. A very detailed recent study of the conductivity of $LiNbO_3$ crystals confirms that the conductivity originates from protons in the temperature range 80–600 °C.[31] The thermal activation energy was determined to be (1.23 ± 0.04) eV in $LiNbO_3$ and (1.17 ± 0.01) eV in $LiNbO_3$:Fe.

However, Williams *et al.* reported a correlation between illumination and the motion of silicon ions in $LiNbO_3$.[24] Therefore Meyer *et al.* performed a theoretical and experimental investigation of thermal fixing in $LiNbO_3$ doped with iron and silicon.[32] In their theoretical approach, the authors neglected the change of the bulk photovoltaic current with changing concentration of optically excitable electrons. Within their model they determined the concentration of ions which is required for the explanation of the fixing process and compared this with the concentrations of silicon and hydrogen; large discrepancies lead to the conclusion that silicon and hydrogen are not responsible for the fixing process. Because of the incomplete modeling, this conclusion is doubtful. Furthermore, there were large uncertainties in the determination of the H^+ concentration.[31] Meyer *et al.* also pointed out that vacancies may contribute to the compensation process.[32] Kovalevich *et al.* reported that in $LiNbO_3$ above 100 °C the light-induced space-charge fields are large enough to create a local polarization reversal.[25] An increased amount of abrupt changes of the diffraction efficiency observed at the end of high-temperature writing was attributed to local polarization changes.[32]

Vormann *et al.* showed that a reduction of the hydrogen concentration lowers the thermal fixing capability of $LiNbO_3$:Fe and that fixing of a macroscopic light pattern yields a slight change in the H^+ concentration.[33] The effect was too small for a quantitative comparison between measured and expected H^+ distributions. In contrast to these results, holographic investigations of thermal fixing in $LiNbO_3$:Cu revealed no significant influence of the concentration of the protons.[34]

To summarize, there are many indications that hydrogen plays an important role in thermal fixing,[35] but until now no unambiguous proof has been achieved. Furthermore, there are indications that local polarization reversals or other effects may occur and contribute to the fixing procedure.

B. Development by homogeneous illumination

The first explanation of the development process was vague: ''optically ionizable traps tend to uniformly redistribute, leaving an electric-field pattern due to the uncompensated charge pattern.''[6] Because the space-charge field is compensated there seems to be no reason for a migration and redistribution of the excited electrons. Kulikov and Stepanov carried out a modeling of the development process.[36] At room temperature holographic recording reaches a stationary condition if drift currents induced by the space-charge field compensate for bulk photovoltaic and diffusion currents. At enhanced temperatures, this space-charge field is compensated and the charge transport continues until the compensation mechanism stops or no more empty or filled electron traps are available. Consequently, a considerably modulated concentration of filled and empty photoionizable traps can be created. Although the development is performed by homogeneous illumination, this spatially modulated impurity concentration gives rise to a modulated current and a spatially inhomogeneous space-charge field. From the ratio of the diffraction efficiencies of the initial and of the fixed hologram the spatially averaged concentration of filled electron traps can be estimated.[36]

Meyer *et al.* performed a more detailed investigation.[32] Bulk photovoltaic currents arise from optical excitations of charge carriers. Because of appreciable changes of the concentration of filled electron traps during the recording process, the bulk photovoltaic current will also change, which was not considered in their theory. The first complete set of basic equations and analytic solutions for recording and development of thermally fixed holograms was presented by Hertel *et al.*[37] Their theory well explained the evolution of magnitude and phase position of a holographic grating during development measured by Matull and Rupp.[38] Carrascosa and Agulló-López additionally considered thermal excitation of the electronic charge carriers[39] which was neglected by Hertel *et al.* There are indications that these excitations are of importance in $LiNbO_3$ for temperatures above 180 °C.[40] This may explain the decrease of the performance of thermal fixing at higher temperatures. Analytic solutions for the time evolutions during fixing and development of gratings for many different situations were obtained by Montemezzani *et al.*[20]

Although these theoretical approaches describe many experimental results, further mechanisms may significantly contribute to the permanent refractive-index changes. Kapphan and Breitkopf determined recently the relation between the H^+ concentration and the refractive-index changes which are directly induced by protons.[41] According to this calibration, even H^+ concentrations which are typical for $LiNbO_3$ bulk material may cause refractive-index changes of about 10^{-4}. Confirmations that the development process is based on a spatially modulated concentration of empty and filled electron traps and that the refractive-index changes result mainly from the electro-optic effect are still missing.

III. EXPERIMENTAL METHODS

A. Crystals

Iron- and copper-doped congruently melting lithium niobate crystals ($LiNbO_3$:Fe, $LiNbO_3$:Cu) are investigated. Table I summarizes dimensions, total iron, copper, and hydrogen concentrations, and the concentration ratios of Fe^{2+}/Fe^{3+} and Cu^+/Cu^{2+} ions. The crystals are labeled with an F or C to indicate iron or copper doping; an H is added if the crystals contain many H^+ ions.

Absorption spectra are measured utilizing a CARY 17D spectrometer. The iron concentrations c_{Fe} are obtained by mass spectroscopy and x-ray fluorescence analysis, and from the absorption coefficients at 477 nm, the Fe^{2+} concentrations $c_{Fe^{2+}}$ are deduced.[42] This yields the Fe^{3+} concentrations $c_{Fe^{3+}}=c_{Fe}-c_{Fe^{2+}}$ and the concentration ratios $c_{Fe^{2+}}/c_{Fe^{3+}}$. The concentrations c_{Cu^+} and $c_{Cu^{2+}}$ of the Cu^+ and Cu^{2+} ions can be derived from the absorption values. Transitions of electrons from Cu^+ into the conduction band cause an absorption band around 365 nm and transition of electrons from Cu^{2+} into an excited state, which is induced by crystal-field splitting, yields an absorption band around

TABLE I. Notations, dimensions, iron, copper, and hydrogen concentrations c_{Fe}, c_{Cu}, and c_{H^+}, and concentration ratios $c_{Fe^{2+}}/c_{Fe^{3+}}$ and $c_{Cu^+}/c_{Cu^{2+}}$ of Fe^{2+}/Fe^{3+} and Cu^+/Cu^{2+} ions of the investigated $LiNbO_3$:Fe and $LiNbO_3$:Cu crystals. The **c** axis of the crystals is parallel to the largest crystal side and in the experiments the light propagates along the shortest dimension.

Label	Dimensions (mm^3)	c_{Fe} (10^{24} m^{-3})	$c_{Fe^{2+}}/c_{Fe^{3+}}$	c_{Cu} (10^{24} m^{-3})	$c_{Cu^+}/c_{Cu^{2+}}$	c_{H^+} (10^{24} m^{-3})
FH1	0.99×4.14×5.10	71	0.04			0.6
FH2	0.99×4.09×5.12	71	0.04			0.6
F	1.07×3.99×5.02	7	0.33			0.09
CH	1.14×4.08×5.12			12	0.77	2.8

1040 nm.[5] Then the overall copper concentrations $c_{Cu} = c_{Cu^+} + c_{Cu^{2+}}$ and the concentration ratios $c_{Cu^+}/c_{Cu^{2+}}$ can be determined. The method has been calibrated by x-ray fluorescence and atomic absorption spectroscopy.[5]

B. Thermal fixing

Macroscopic Gaussian intensity distributions are thermally fixed in the $LiNbO_3$ crystals. The fixing experiments are carried out at a temperature of 163 °C (absolute accuracy ±3 °C, stability better than ±0.1 °C). For illumination, ordinarily polarized light of an argon-ion laser (wavelength 514 nm) is used.

Different light patterns are utilized: The $LiNbO_3$:Fe sample FH1 is illuminated by an unexpanded laser beam of circularly Gaussian-shaped intensity distribution ($1/e^2$ diameter: 2.1 mm). Light intensity in the center of the Gaussian pattern and exposure time are 580 kW m^{-2} and 311 h, respectively. The $LiNbO_3$:Fe crystal FH2 is illuminated by the same light pattern for about 315 h, but without external electrical heating.

The $LiNbO_3$:Fe sample F and the $LiNbO_3$:Cu sample CH are illuminated by one-dimensional Gaussian intensity patterns ($1/e^2$ widths: 1.0 and 1.1 mm, respectively). This light distribution is achieved by expansion of the laser beam to a diameter of 30 mm and subsequent focusing onto the crystal with a cylindrical lens (focal length: 300 mm). The Gaussian intensity profile is oriented parallel to the **c** axis of the crystals; the intensity inhomogeneities perpendicular to the **c** axis are less than 2%. Light intensity in the center of the Gaussian pattern and exposure time are 400 kW m^{-2} and 89 h for the sample F, and 360 kW m^{-2} and 47 h for the crystal CH.

After illumination, the crystals are cooled to room temperature within 30 min. By homogeneous incoherent illumination with white light of a halogen lamp, the refractive-index patterns are developed until no further changes of the refractive indices are observed. The intensity of the development light is typically 1 kW m^{-2}.

C. Absorption topography

1. Visible light: Fe^{2+} and Cu^+ concentrations

As mentioned earlier, the concentrations $c_{Fe^{2+}}$ and c_{Cu^+} of Fe^{2+} and Cu^+ ions, respectively, can be directly determined by absorption measurements. From the absorption coefficient $\alpha_{477\,nm}$ of ordinarily polarized light of 477 nm wavelength the concentrations are ascertained according to the relations $c_{Fe^{2+}} = 2.2\times10^{21}\ m^{-2}\ \alpha_{477\,nm}$ for $LiNbO_3$:Fe (Ref. 42) and $c_{Cu^+} = 2.0\times10^{21}\ m^{-2}\ \alpha_{477\,nm}$ for $LiNbO_3$:Cu (Ref. 5).

Topographic absorption measurements are performed utilizing a weak ordinarily polarized argon-ion laser beam (wavelength 477 nm) which is spatially filtered and focused. The focal length of the lens, $1/e^2$ diameter of the beam at the focal point, and light power are 300 mm, 70 μm, and 3 μW. A photodiode behind the crystal monitors the transmitted light intensity and the absorption coefficient $\alpha_{477\,nm}$ is determined considering reflection losses. A translation stage moves the crystal parallel to the **c** axis. With this setup, spatially resolved measurements of $\alpha_{477\,nm}$ with a resolution better than 70 μm and an accuracy of about ±3 m^{-1} are performed.

2. Infrared light: H^+ concentration

In $LiNbO_3$ hydrogen yields a pronounced absorption at 2870 mm because of OH^- stretching vibrations.[29] This absorption can be measured with high accuracy. The proton concentration in proton-exchanged waveguides is well known[43] which enables a calibration of the absorption measurements. The most accurate relation available from the literature is $c_{OH^-} = c_{H^+} = (1.67\pm0.09)\times10^{22}\ m^{-2}\ \alpha_{2870\,nm}$ (Ref. 41), where $c_{OH^-} = c_{H^+}$ is the hydrogen concentration and $\alpha_{2870\,nm}$ is the absorption coefficient at the maximum of the OH^- absorption. An objection against this calibration method of OH^- absorption might be that the OH^- absorption is different in highly proton-exchanged waveguides and bulk material. However, by thermal annealing a large fraction of the protons diffuses into the bulk material. This yields a change of the center wavelength, but no change of width and magnitude of the OH^- absorption band,[41,44] verifying that the relation is also valid for bulk material. This calibration is in perfect agreement with other literature values where proton-exchanged waveguides were also investigated.[31,44]

For the infrared absorption measurements, a Fourier spectrometer (Bruker HR120) is used. A slit of 110 μm width is inserted, and the crystal is mounted on a translation stage. By looking for the height of the OH^- absorption band and comparison with the baseline we take into account reflection losses. With this setup, spatially resolved measurements of $\alpha_{2870\,nm}$ with a resolution of 110 μm and an accuracy of about ±0.5 m^{-1} are carried out.

D. Refractive-index topography

Spatially resolved measurements of refractive index are performed with a Mach-Zehnder interferometer. The setup is

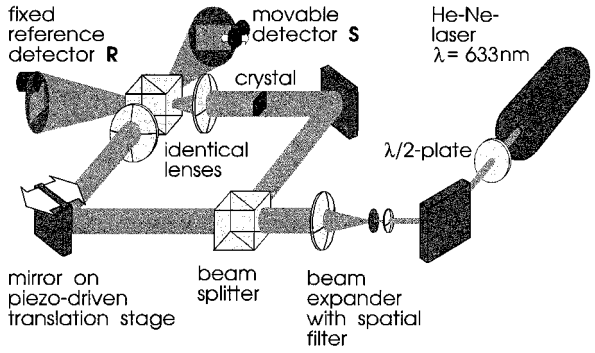

FIG. 1. Schematic diagram of the setup used for spatially resolved measurements of the refractive-index changes created by thermal fixing. Phase changes are induced by the crystal and detected by a Mach-Zehnder interferometer. A reference detector enables consideration of phase drifts and noise; details are described in the text.

shown schematically in Fig. 1. Light of a helium-neon laser (wavelength $\lambda = 633$ nm) passes a rotatable half-wave plate which enables adjustment of light polarization. After expansion and spatial filtering the beam enters the Mach-Zehnder interferometer. By a piezoelectrically supported mirror in one of the interferometer arms the relative phase ϕ_0 of the two interferometer beams can be changed. The crystal is positioned in one arm of the interferometer and a lens images the back face of the sample onto the detection plane (about eight times magnification). An identical lens is required in the second interferometer arm in order to obtain the appropriate reference wave. Without a sample, interference of the beams in the detection planes yields a homogeneous intensity distribution; with the sample, fringes may appear which originate from phase changes induced by the crystal. Some samples are slightly wedged in order to reduce the influence of Fabry-Pérot interferences on holographic experiments. The created homogeneous fringe pattern is easily compensated by readjustment of the lens position. Photodiodes behind small apertures (diameters used are 30–200 μm) measure the light intensities I_S and I_R of a signal and of a reference in the detection planes (see Fig. 1). The signal detector is mounted together with the aperture on a translation stage and can be moved along the **c** axis of the crystal. The reference detector is positioned outside the image of the crystal. The following procedure is carried out at each position X of the movable detector in the detection plane. The

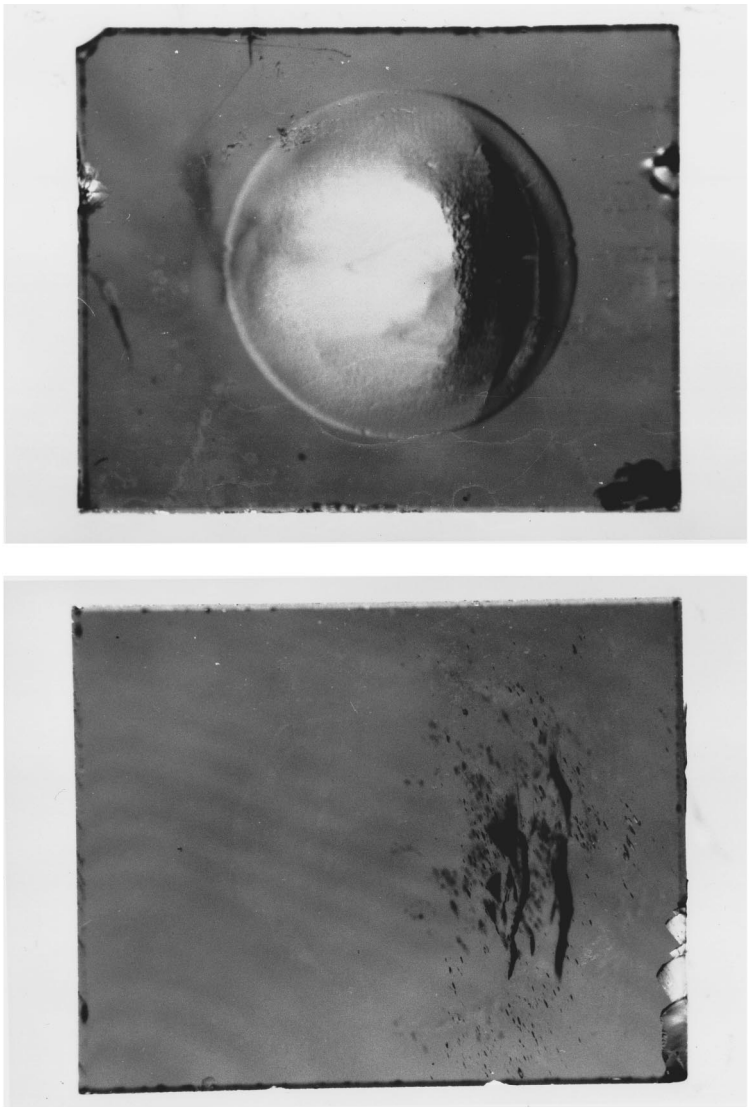

FIG. 2. Top: Photograph of the $LiNbO_3$:Fe crystal FH1 after 311 h illumination at a temperature of 163 °C with an ordinarily polarized two-dimensional Gaussian light beam. Wavelength, full $1/e^2$ width, and center intensity of the beam are 514 nm, 2.1 mm, and 580 kW m^{-2}. Bottom: Photograph of the $LiNbO_3$:Fe crystal FH2 after 315 h illumination under the same conditions, but without external electrical heating. By absorption of light the temperature of the sample is increased to about 40 °C. In both photographs the **c** axis of the crystals points from the left to the right side.

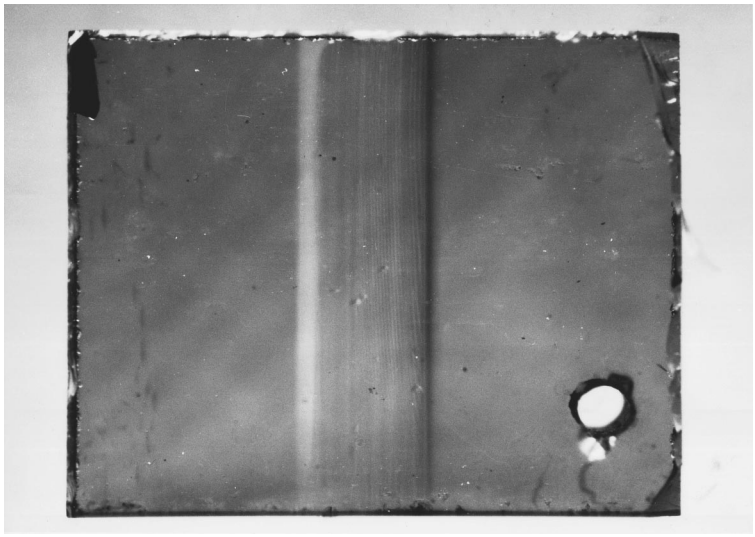

FIG. 3. Photograph of the $LiNbO_3$:Fe crystal F after 89 h illumination at a temperature of 163 °C with an ordinarily polarized light beam. The light pattern has an one-dimensional Gaussian shape. Wavelength, full $1/e^2$ width, and center intensity of the beam are 514 nm, 1.0 mm, and 400 kW m^{-2}. The light pattern is slightly modified by Fabry-Pérot interferences resulting from internal reflections. The **c** axis of the crystal points from the left to the right side. The crystal has a hole in the lower right region.

interferometer phase ϕ_0 is shifted by the piezoelectrically supported mirror in 50 steps of about 0.25 rad and the intensities $I_S(\phi_0,X)$ and $I_R(\phi_0)$ are recorded. Sinusoidal fits of $I_S=I_{S,0}\sin[\phi_0+\phi_S(X)]$ and $I_R=I_{R,0}\sin(\phi_0+\phi_R)$ to the two data sets yield the phases $\phi_S(X)$ and ϕ_R. The difference $\Delta\phi(X)=\phi_S(X)-\phi_R$ is the phase change introduced by the crystal modulo multiples of 2π. We define $\Delta\phi$ to be zero in the sample near the crystal edge; scanning along the image of the crystal yields $\Delta\phi(X)$ which arises from the refractive-index profile $\Delta n(X)=\lambda\Delta\phi(X)(2\pi d)^{-1}$, where d is the crystal thickness. Jumps of $\Delta\phi$ occur if the phase changes exceed 2π; this is taken into account and the $\Delta\phi$ values are continuously connected. The obtained Δn curve must reach zero near the other boundary of the crystal if the continuation procedure is correct. The refractive-index profile $\Delta n(x)$, where x is the spatial position on the crystal, is deduced from $\Delta n(X)$ with the known magnification factor. A complete scan requires between 30 min and 8 h, depending on the resolution used. Interferometer instabilities, e.g., a slow thermal movement of mirrors, cannot affect the measurements because we look for the phase difference $\phi_S-\phi_R$.

There are three different resolutions which determine the fidelity of this setup: The minimum phase change which can be detected, the maximum gradient of phase changes which can be resolved, and the spatial resolution. (1) Without light-induced refractive-index changes the $|\Delta\phi|$ values are smaller than 0.03 rad for all positions x. Thus the smallest detectable phase change and refractive-index changes are 0.03 rad and 3×10^{-6} for $d=1$ mm. (2) The difference of the phase changes $\Delta\phi$ at two neighboring positions must be below 2π; otherwise complete fringes may be overlooked by movement of the detector to the next position. This determines a maximum gradient of the profiles which can be detected. Considering the magnification by the lenses we can resolve 1 rad μm^{-1} which corresponds to a maximum refractive-index gradient of 10^{-4} μm^{-1} for $d=1$ mm. (3) Because of the imaging system and the signal detector aperture, spatial resolutions between 4 and 25 μm are achieved.

IV. EXPERIMENTAL RESULTS

Figure 2 shows photographs of the $LiNbO_3$:Fe samples FH1 and FH2 after illumination. The direction of the **c** axis is determined by the pyroelectric effect; after heating, the left side is positively charged and the right side is negatively charged. Thus the **c** axis points from the left to the right side. After some seconds, surface charge compensates for the changes of the spontaneous polarization.

The sample FH1, which is illuminated at a temperature of 163 °C, shows a strong change of color. The crystal is bleached in the illuminated region and a dark arc appears in

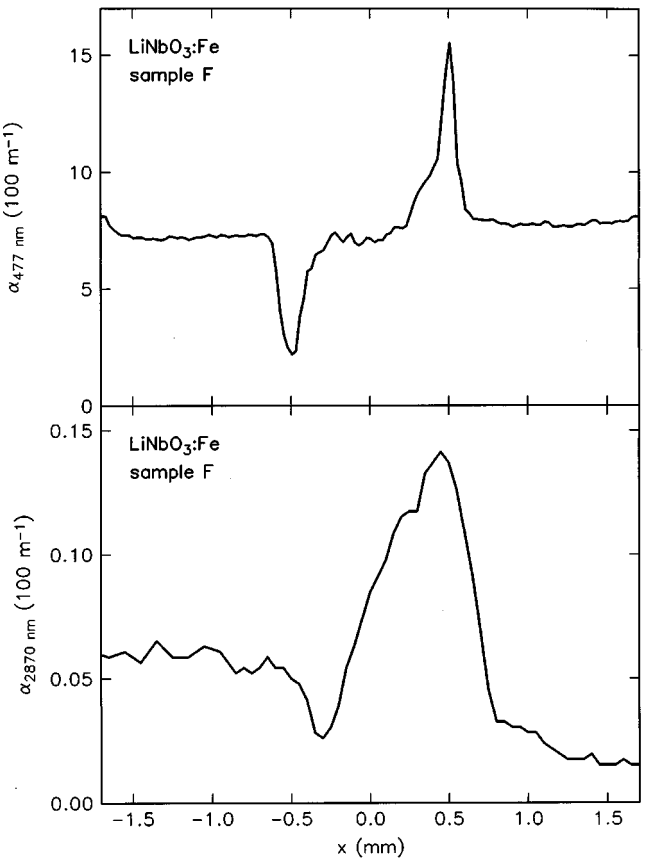

FIG. 4. Absorption coefficients $\alpha_{477\,nm}$ and $\alpha_{2870\,nm}$ for ordinarily polarized light of 477 and 2870 nm wavelengths vs spatial coordinate x along the **c** axis of the $LiNbO_3$:Fe crystal F after thermal fixing of a macroscopic Gaussian intensity pattern.

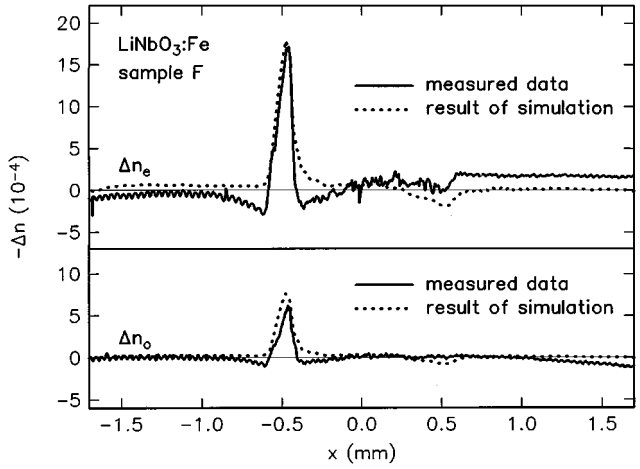

FIG. 5. Changes of the refractive index for ordinarily and extraordinarily polarized light, Δn_o and Δn_e, vs spatial coordinate x along the **c** axis of the $LiNbO_3$:Fe crystal F after thermal fixing and development of a macroscopic Gaussian intensity pattern. The solid curve represents measured data and the dotted curve results from computer simulations.

the $+c$ direction. The FH2 sample is illuminated without external heating, but light absorption increases the crystal temperature to 40 °C. However, no absorption changes are created; the illumination procedure causes only mechanical defects. During illumination the speckle pattern behind the crystal shows an interesting behavior: A slow continuous movement followed by a rapid jump to the original position and so on. At 163 °C (sample FH1) the effect is present only during the first minutes of illumination and the frequency of the periodic movement is about 1 Hz. At 40 °C (sample FH2) the effect appears during the whole illumination time; the frequency is about 4 Hz.

A photograph of the $LiNbO_3$:Fe sample F after illumination is shown in Fig. 3. A bleached and a darkened stripe appear in the $-c$ and $+c$ directions. The maximum of the one-dimensional Gaussian intensity pattern was in the middle between these stripes. Figure 4 shows the corresponding absorption profiles and Fig. 5 illustrates the refractive-index changes after development, i.e., homogeneous illumination of this crystal.

Figure 6 shows that, after illumination, the $LiNbO_3$:Cu crystal CH also has a bleached and a darkened stripe in the $-c$ and $+c$ directions. The corresponding absorption profiles and the refractive-index changes after development are shown in the Figs. 7 and 8.

V. COMPUTER SIMULATIONS

In this section, computer simulations of recording and development processes are described. The aim is to check whether the model of electron redistribution and ionic space-charge field compensation can explain the measured data quantitatively.

A. Basic equations

For rate, current, continuity, and Poisson equations we write in one-dimensional approach:

$$\frac{dc_{D^-}}{dt} = -qSIc_{D^-} + r(c_D - c_{D^-})n, \tag{1}$$

$$j_e = e\mu_e nE + \beta^* c_{D^-} I + k_B T \mu_e \frac{\partial n}{\partial x}, \tag{2}$$

$$j_i = e\mu_i c_i E - k_B T \mu_i \frac{\partial c_i}{\partial x}, \tag{3}$$

$$\frac{dj_e}{dx} + \dot{\rho}_e = 0, \tag{4}$$

$$\rho_e = -e(n + c_{D^-} - c_{D^-,0}), \tag{5}$$

$$\frac{dj_i}{dx} + \dot{\rho}_i = 0, \tag{6}$$

$$\rho_i = +e(c_i - c_{i,0}), \tag{7}$$

$$\frac{dE}{dx} = (\rho_e + \rho_i)(\epsilon\epsilon_0)^{-1}, \tag{8}$$

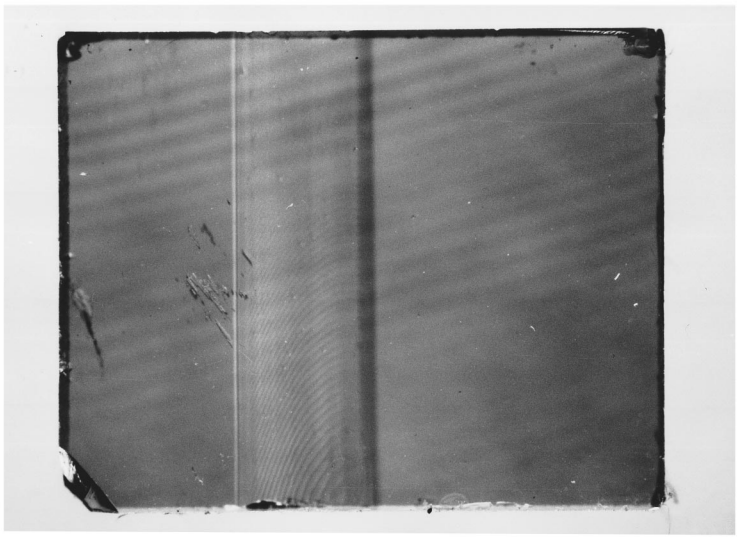

FIG. 6. Photograph of the $LiNbO_3$:Cu crystal CH after 47 h illumination at a temperature of 163 °C with an ordinarily polarized light beam. The light pattern has an one-dimensional Gaussian shape which is slightly modified by Fabry-Pérot interferences resulting from internal reflections. Wavelength, full $1/e^2$ width, and center intensity of the beam are 514 nm, 1.1 mm, and 360 kW m^{-2}. The **c** axis of the crystal points from the left to the right side.

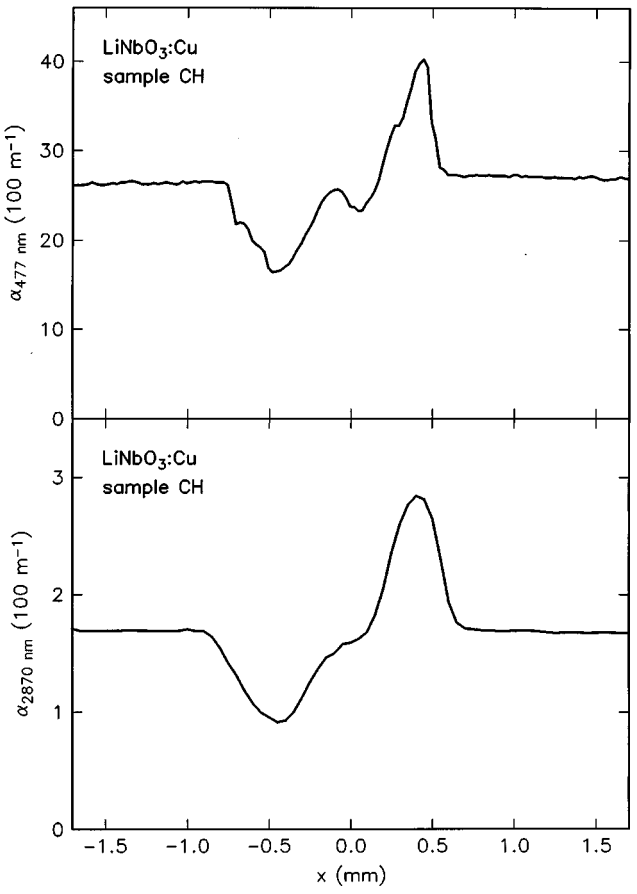

FIG. 7. Absorption coefficients $\alpha_{477\,\mathrm{nm}}$ and $\alpha_{2870\,\mathrm{nm}}$ for ordinarily polarized light of 477 and 2870 nm wavelengths vs spatial coordinate x along the **c** axis of the $LiNbO_3$:Cu crystal CH after thermal fixing of a macroscopic Gaussian intensity pattern.

where c_{D^-} is the concentration of traps filled with an electron, e.g., $c_{Fe^{2+}}$ in $LiNbO_3$:Fe and c_{Cu^+} in $LiNbO_3$:Cu; c_D is the concentration of the sum of filled and empty traps, e.g., c_{Fe} in $LiNbO_3$:Fe and c_{Cu} in $LiNbO_3$:Cu; q is the quantum efficiency for excitation of an electron from a filled trap into the conduction band upon absorption of a photon; S is the photon absorption cross section; I is the light intensity in photons per square meter and second; r is the recombination coefficient; n is the density of electrons in the conduction band; j_e is the electron current density; e is the elementary charge; μ_e is the electron mobility; E is the electric field; β^* is the bulk photovoltaic coefficient; k_B is Boltzmann's constant; T is the temperature; x is the spatial coordinate along the **c** axis of the crystal; j_i is the ion current density; ρ_e is the charge density of redistributed electrons; μ_i is the ion mobility; c_i is the ion concentration, $c_{D^-,0}$ is the spatially averaged concentration of filled electron traps; ρ_i is the charge density of redistributed ions; $c_{i,0}$ is the spatially averaged ion concentration; ϵ is the dielectric constant; and ϵ_0 is the permittivity of free space. A dot indicates the time derivative and from all vector quantities only the x component occurs. The one-dimensional approach is useful for simulations of, e.g., illuminations with one-dimensional Gaussian patterns or holographic gratings.

Thermal excitations of electrons from the filled traps into the conduction band are neglected in Eq. (1); appreciable contributions are expected only for temperatures above 180 °C.[40] Drift, bulk photovoltaic effect, and diffusion contribute to the electron current [Eq. (2)]. The ionic current originates from drift and diffusion [Eq. (3)]; no bulk photovoltaic effect is considered because the ions are not photoionized. Two continuity equations [Eqs. (4) and (6)] guarantee electron and ion conservation. In the initial situation, overall charge neutrality is maintained by nonmobile compensation charges. This is taken into account by the terms $c_{D^-,0}$ and $c_{i,0}$ in Eqs. (5) and (7).

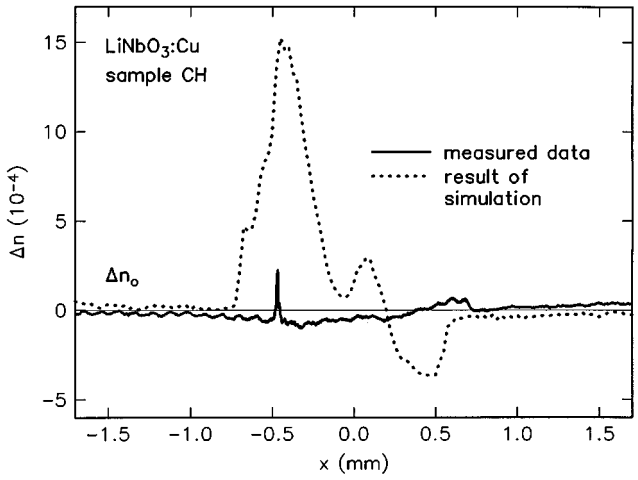

FIG. 8. Changes of the refractive-index for ordinarily polarized light Δn_o vs spatial coordinate x along the **c** axis of the $LiNbO_3$:Cu crystal CH after thermal fixing and development of a macroscopic Gaussian intensity pattern. The solid curve represents measured results and the dotted curve results from computer simulations.

Equations (1), (4), and (5), and the adiabatic approximation,[45] i.e., neglection of $\dot{n}$, yield the density of electrons in the conduction band

$$n=\frac{1}{er(c_D-c_{D^-})}\frac{dj_e}{dx}+\frac{qSI}{r}\frac{c_{D^-}}{c_D-c_{D^-}}, \tag{9}$$

where n follows instantaneously the changing distribution of the electron current and the changing concentrations of filled and empty electron traps.

B. Algorithm

Previous models often utilized Fourier development of the spatially dependent quantities.[20,37,39] Neglection of higher-order Fourier components enables analytic solution of the equations; formulas for the evolutions of the charge carrier concentrations and of the space-charge field during fixing and development procedures were derived. For Gaussian-shaped intensity distributions Fourier development to first order is not applicable; also in holographic experiments it is doubtful whether Fourier development is appropriate. The thermal fixing process reaches the steady-state situation, if all available ions are redistributed or if there are no more filled or empty electron traps; nonsinusoidal steady-state concentration distributions might be created.

We solve Eqs. (2)–(9) in space by dividing the crystal along the x direction into 1024 sections. For computer simulation of the *recording process*, the initial values are first calculated (no light, spatially homogeneous c_{D^-} and c_i). Then, the following algorithm is used. (1) Calculation of the current densities j_e and j_i [Eqs. (2), (3), and (9)]. (2) Computation of the D^- and ion distributions which are changed because of the currents which redistribute charge during the time interval dt [Eqs. (4)–(7)]. (3) Calculation of the resulting space-charge field [Eq. (8)]. Then the procedure is repeated for the next time step dt and so on. The time interval dt is chosen to be so small that further reduction of dt yields no changes of the computed results. On a Pentium PC about 8 h were required for simulation of a 50 h recording experiment. For simulation of the *development process* the measured concentration profiles c_{D^-} are used and then, by the algorithm described above, the steady-state space-charge field is calculated. At room temperature, where the ions are practically immobile, the steady-state situation is reached after the dielectric relaxation time $\epsilon\epsilon_0/\sigma$, where σ is the photoconductivity. Thus the development can be simulated within a few minutes.

C. Material parameters

Fortunately, $LiNbO_3$ has been intensively investigated which enables determination of the charge transport parameters. The total concentrations of filled and empty electron traps ($c_D = c_{Fe}, c_{Cu}$), and the spatially averaged concentration of hydrogen ($c_{H^+,0}$) are already presented in Table I. Together with the concentration ratios $c_{Fe^{2+}}/c_{Fe^{3+}}$ and $c_{Cu^+}/c_{Cu^{2+}}$ given in Table I, the spatially averaged concentrations of filled-electron traps ($c_{Fe^{2+},0}, c_{Cu^+,0}$) are also known.

Because of large concentrations of c_{D^-}, the first term on the right-hand-side of Eq. (9) is many orders of magnitude smaller than the second term. The computer simulations are performed considering the complete Eq. (9), but because the first term is negligible, only the value of the electronic conductivity $\sigma_e = e\mu_e n \propto \mu_e q S r^{-1}$ has significant influence on the computer simulations; variation of the parameters μ_e, q, S, and r yields no changes of the results if $\mu_e q S r^{-1}$ is always the same. Equation (9) yields $\sigma_e = e\mu_e q S I r^{-1} c_{D^-}(c_D - c_{D^-})^{-1}$ for homogeneous illumination. Utilizing this relation, the parameter $\mu_e q S r^{-1}$ can be determined from published photoconductivity data. Holographic erasure experiments in as-grown and thermally annealed $LiNbO_3$:Fe and $LiNbO_3$:Cu crystals were performed yielding the conductivity values.[34,46] The relations $\sigma_e \propto I$ and $\sigma_e \propto [c_{D^-}(c_D - c_{D^-})^{-1}]$ were confirmed and from the measured data the coefficient $\mu_e q S r^{-1} = 2.0\times10^{-14}$ mV^{-1} for $LiNbO_3$:Fe (light wavelength 514 nm) and $\mu_e q S r^{-1} = 1.0\times10^{-15}$ mV^{-1} for $LiNbO_3$:Cu (light wavelength 488 nm) are obtained.

The bulk photovoltaic coefficient for photoexcitation of electrons from Fe^{2+} is $\beta^* = 1.8\times10^{-51}$ m^3 A s (light wavelength 514 nm, Ref. 47). The bulk photovoltaic coefficient β^* for photoexcitation of electrons from Cu^+ into the conduction band is determined from data published in Ref. 34, where the saturation value $|\Delta n_s|$ of the amplitude of the refractive-index grating was measured. Considering $|\Delta n_s| = |n_o^3 r_{113} E_{sc}/2|$ with $E_{sc} = j_{phv}/\sigma_e$ and $j_{phv} = \beta^* c_{Cu^+} I$, where n_o is the ordinary refractive index, r_{113} is the corresponding electro-optic coefficient, E_{sc} is the space-charge field, and j_{phv} is the bulk photovoltaic current density, we get $j_{phv}(c_{Cu^+}I)^{-1} = \beta^* = 1.0\times10^{-52}$ m^3 A s (light wavelength 488 nm). Here $n_o = 2.3486$ and $r_{113} = 12\times10^{-12}$ m V^{-1} are used (light wavelength 488 nm).[48–50] Furthermore, we checked β^* of $LiNbO_3$:Cu by direct measurement of the bulk photovoltaic current densities for different light intensities and confirmed the value of 10^{-52} m^3 A s.

It has been reported that doping increases the proton mobility,[31] perhaps because of filled traps. Fortunately, experiments were performed with a $LiNbO_3$ crystal containing the same concentration of transition-metal ions as the $LiNbO_3$:Cu sample CH used in our investigation; according to Ref. 31 we can write for the ionic mobility $\mu_i = eD_0(k_BT)^{-1}\exp[-E_A(k_BT)^{-1}]$ with $eD_0k_B^{-1} = 3.31$ m^2 K V^{-1} s^{-1} and $E_A = 1.17$ eV. For the temperatures 20 and 163 °C, proton mobilities of 8.3×10^{-23} and 2.2×10^{-16} m^2 V^{-1} s^{-1} are deduced. The dielectric constant of $LiNbO_3$ is $\epsilon_{33} = 28$.[51,52] Tables II and Tables III summarize the relevant material parameters of $LiNbO_3$:Fe and $LiNbO_3$:Cu.

TABLE II. Parameters used for computer simulation of hologram development at room temperature in the $LiNbO_3$:Fe sample F: $c_D = c_{Fe}$, sum of the concentrations of filled and empty electron traps; $c_{D^-,0}$, spatially averaged concentration of filled electron traps $D^- = Fe^{2+}$; μ_e, electron mobility; q, quantum efficiency for excitation of an electron upon absorption of a photon; S, photon absorption cross section; r, recombination coefficient; β^*, bulk photovoltaic coefficient; $c_{i,0}$, spatially averaged concentration of hydrogen ions H^+; μ_i, mobility of hydrogen ions (temperature $T = 20$ °C).

c_D	7.0×10^{24} m^{-3}
$c_{D^-,0}$	1.7×10^{24} m^{-3}
$\mu_e q S r^{-1}$	2.0×10^{-14} m V^{-1}
β^*	1.8×10^{-51} m^3 A s
$c_{i,0}$	0.9×10^{23} m^{-3}
μ_i ($T = 20$ °C)	8.3×10^{-23} m^2 V^{-1} s^{-1}

TABLE III. Parameters used for computer simulation of recording at enhanced temperature and of development at room temperature in the $LiNbO_3$:Cu crystal CH: $c_D = c_{Cu}$, sum of the concentrations of filled and empty electron traps; $c_{D^-,0}$; spatially averaged concentration of filled electron traps $D^- = Cu^+$; μ_e, electron mobility; q, quantum efficiency for excitation of an electron upon absorption of a photon; S, photon absorption cross section; r, recombination coefficient; β^*, bulk photovoltaic coefficient; $c_{i,0}$, spatially averaged concentration of hydrogen ions H^+; μ_i, mobility of hydrogen ions (recording temperature $T = 163$ °C, development temperature $T = 20$ °C).

c_D	1.2×10^{25} m^{-3}
$c_{D^-,0}$	5.2×10^{24} m^{-3}
$\mu_e q S r^{-1}$	1.0×10^{-15} m V^{-1}
β^*	1.0×10^{-52} m^3 A s
$c_{i,0}$	2.8×10^{24} m^{-3}
μ_i ($T = 20$ °C)	8.3×10^{-23} m^2 V^{-1} s^{-1}
μ_i ($T = 163$ °C)	2.2×10^{-16} m^2 V^{-1} s^{-1}

Some of the parameters are determined from measurements with light of 488 nm wavelength, because no other data are available. It has been shown earlier that the charge transport parameters, e.g., the bulk photovoltaic coefficients, do not depend on the proton concentration.[53]

Refractive indices and electro-optic coefficients are required to calculate the refractive-index changes from the computed space-charge fields. The refractive-index distribution is measured with light of 633 nm wavelength and the appropriate refractive indices, and electro-optic coefficients for ordinarily and extraordinarily polarized light are $n_o = 2.2864$, $n_e = 2.2025$, $r_{113} = 10.9 \times 10^{-12}$ m V^{-1}, and $r_{333} = 34 \times 10^{-12}$ m V^{-1}.[48,49]

VI. DISCUSSION

A. Changes of the crystal color

During illumination, electrons are excited from filled electron traps (Fe^{2+} or Cu^{+}) into the conduction band, and they move because of the bulk photovoltaic effect in the $+c$ direction of the crystal. Later they are captured by empty electron traps (Fe^{3+} or Cu^{2+}). Because absorption in the visible originates from the filled electron traps (Fe^{2+} or Cu^{+}), the $-c$ region, where the electrons come from, is bleached and the $+c$ region, where the electrons are trapped, is darkened.

The largest space-charge fields obtained in $LiNbO_3$ crystals are typically about $E = 10^7$ V m^{-1} (Ref. 4). For a rough estimation of the charge redistribution required to build up this space-charge field, we use the model of a capacitor. The area charge density $Q/A = \epsilon\epsilon_0 E$ yields the space-charge field E. The required density of redistributed charge carriers is $\epsilon\epsilon_0 E (we)^{-1}$, where w is the width of the regions, where the electrons are accumulated, or where they come from. With w of about 0.1 mm and $\epsilon = 28$ (Refs. 51 and 52) we get 10^{20} m^{-3}. Such a change of the Fe^{2+} concentration will yield only absorption changes of 0.05 m^{-1} (Sec. III C 1). This is the reason why in sample FH2, which is illuminated at 40 °C, no appreciable absorption changes are created. However, at 163 °C, obviously the space-charge fields become compensated and much more charge is redistributed. The charge redistribution stops only if there are no more empty or filled electron traps.

The iron concentrations of the samples FH1 and FH2 are very large. Thus large space-charge fields build up until breakdown occurs; this explains the periodic movement of the speckle pattern behind the crystal. Build-up of the space-charge field yields a continuous slow movement of the speckle pattern and breakdown of the field causes an abrupt jump of the pattern. The frequency of this process is lowered at enhanced temperatures, because build-up of the space-charge field is slowed down by a charge compensation mechanism. Obviously, the mechanical defects observed in the crystal FH2, after illumination, are created by the large number of internal breakdowns of the space-charge field. The magnitude of the space-charge field after a breakdown is not known and cannot be simply calculated. Thus computer simulations of the processes in these crystals are difficult.

B. Charge compensation mechanism

From the spatially resolved measurements of the absorption coefficients at 477 and 2870 nm (Fig. 4), the concentration profiles of filled electron traps and of hydrogen are calculated (Secs. III C 1 and III C 2). Figure 9 shows the light-induced concentration changes of Fe^{2+} and H^{+} in the $LiNbO_3$:Fe crystal F after the fixing experiment. Obviously, there are not enough protons to compensate for the redistribution of electrons; thermal fixing without protons occurs.

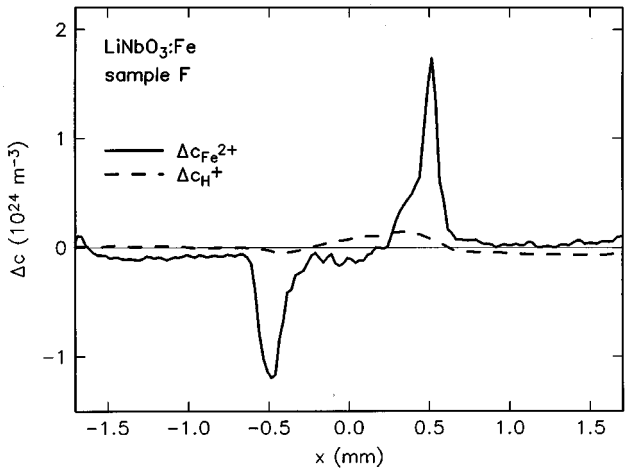

FIG. 9. Changes of the Fe^{2+} and H^{+} concentrations, $\Delta c_{Fe^{2+}}$ and $\Delta c_{H^{+}}$, vs spatial coordinate x along the **c** axis of the $LiNbO_3$:Fe crystal F after thermal fixing of a macroscopic Gaussian intensity pattern. The curves are deduced from absorption measurements.

The following estimation shows that a partial depolarization of the crystal cannot be the origin of compensation. Using once more a capacitor as a model of the system, we get the relation $\epsilon\epsilon_0 E = D = Q/A - \Delta P_s$, where D is the dielectric displacement, Q/A is the area charge density, and ΔP_s is the change of the spontaneous polarization. Integration of $e c_{Fe^{2+}}$ in the region of electron accumulation (Fig. 9), where e is the elementary charge, yields an estimate for Q/A of about $e \times 2 \times 10^{24}$ m$^{-3} \times 10^{-4}$ m ≈ 30 A s m^{-2}. To obtain $E = 0$ this must be compensated by ΔP_s. However, the complete spontaneous polarization of $LiNbO_3$ amounts only 0.7 A s m^{-2} (Ref. 54). Furthermore, as described below, the refractive-index profiles reveal that there is no appreciable depolarization of the crystals. Therefore, changes of the spontaneous polarization can be unambiguously ruled out as the origin of the charge compensation mechanism in thermal fixing experiments with $LiNbO_3$. Charge compensation is achieved by movement of ions or of crystal defects; e.g., moving vacancies or Li^{+} atoms may compensate the space-charge fields. Further investigations are required to identify the compensation mechanism in crystals with small proton concentrations.

The sample FH1 contains more protons and also for this crystal spatially resolved measurements of the concentration changes of Fe^{2+} and H^{+} ions are performed. In this crystal, these concentration changes agree fairly well and hydrogen is responsible for the charge compensation.

The $LiNbO_3$:Cu crystal CH also contains many H^{+} ions. From the $\alpha_{477\,nm}$ and $\alpha_{2870\,nm}$ absorption profiles (Fig. 7) the concentration changes $\Delta c_{Cu^{+}}$ and $\Delta c_{H^{+}}$ of Cu^{+} and H^{+} ions are determined (Secs. III C 1 and III C 2). Figure 10 shows the results and reveals that in this crystal the changes of the Cu^{+} concentrations are compensated by a corresponding

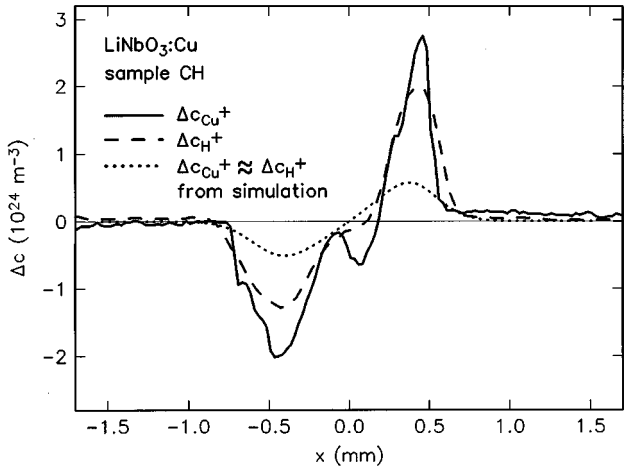

FIG. 10. Changes of the Cu^+ and H^+ concentrations, Δc_{Cu^+} and Δc_{H^+}, vs spatial coordinate x along the **c** axis of the $LiNbO_3$:Cu crystal CH after thermal fixing of a macroscopic Gaussian intensity pattern. Solid and dashed curves are deduced from absorption measurements and the dotted curve results from computer simulations.

proton redistribution; the concentration changes Δc_{Cu^+} and Δc_{H^+} agree rather well, if we take into account uncertainties of the correlation factors between absorption coefficients and concentrations. The H^+ concentration is increased in the region where electrons are accumulated; this is a proof that indeed hydrogen, and not OH^- molecules, migrate in the crystals.

Furthermore, the computer simulation with the parameters of Table III describes fairly well the measured data. Please note that all parameters for the simulation are known from other measurements; there are no fit parameters. If we, e.g., decrease $\mu_e q S r^{-1}$ and increase β^* by a factor of 2, very good agreement with the measured data is achieved. The parameters $\mu_e q S r^{-1}$ and β^* listed in Table III are deduced from room temperature measurements; at 163 °C they may be slightly different. However, the uncertainty of the parameters is only about a factor of two and especially the ionic mobility seems to be correct.

C. Refractive-index changes

In Fig. 5 measured and simulated refractive-index profiles for the $LiNbO_3$:Fe crystal F are shown. The computer simulations utilize the measured concentration profile $c_{Fe^{2+}}(x)$ and the parameters of Table II. The refractive-index changes are excellently described by the simulation, confirming that indeed the development process is due to spatially modulated concentrations of filled and empty electron traps. The different refractive-index changes for extraordinarily and ordinarily polarized light are explained by the same space-charge field considering the different refractive indices and electro-optic coefficients. Refractive-index changes originating from other effects are obviously negligible. There is no appreciable depolarization of the crystals; otherwise the measured refractive-index changes would be smaller.

Figure 8 shows measured and computer-simulated refractive-index profiles for the $LiNbO_3$:Cu crystal CH. For the simulation the measured concentration profile $c_{Cu^+}(x)$ and the parameters of Table III are used. Obviously, the measured refractive-index changes are much smaller than the computed ones.

The space-charge field amplitude depends on the concentration of empty electron traps, i.e., in $LiNbO_3$:Fe and $LiNbO_3$:Cu on Fe^{3+} and Cu^{2+} concentration, respectively.[34,46] Table I shows that the sample F has the smallest concentration of empty electron traps. The computer simulations yield in this crystal for the largest space-charge field 50 kV cm^{-1}. This is below the breakdown field which is about 100 kV cm^{-1}. In the other samples CH, FH1, and FH2 much larger space-charge fields are calculated, e.g., 300 kV cm^{-1} for sample CH. Thus, most probably, in these crystals, breakdowns during development occur and this is the reason that the measured refractive-index changes are much smaller than the calculated ones.

One might argue that in the sample CH other defects than Cu contribute to the charge transport. However, from detailed experiments at room temperature it is known that in copper-doped $LiNbO_3$ crystals the copper ions play a dominant role and that contributions of other defects to the charge transport are negligible.[5,34]

D. Lifetime of holograms

Our results confirm the proton mobility values deduced from the data published in Ref. 31; thermal activation energy and pre-exponential factor of the temperature dependence of the proton mobility seem to be very reliable. It follows that at room temperature the proton mobility is 2.6×10^6 times smaller than at 163 °C (Table III). For the recording of the intensity pattern in the crystal CH about 47 h were required. Considering that the recording time depends on the amount of charge which must be transported from the bright into the dark regions, the recording time scales linearly with the width or period length of the intensity pattern. Therefore, in holographic experiments the recording time of a grating with a period length of 1 μm will be about 3 min. Then the lifetime of the hologram under illumination (continuously developed) is just 3 min multiplied with 2.6×10^6 min $\approx$15 years. In the dark the lifetime is much larger because the space-charge field is compensated and the redistribution of protons stops. The proton concentration is comparable with the concentration of filled electron traps (Table III), which is expected to be optimal for the hologram lifetime.

However, as we demonstrated, another compensation mechanism occurs in crystals with low proton concentration (Sec. VI B). Thus, most probably, in such crystals the lifetime of holograms, even under continuous illumination, is enlarged.

VII. SUMMARY AND CONCLUSIONS

Heating a photorefractive crystal during or after holographic recording and subsequent homogeneous illumination yields fixed refractive-index patterns. This procedure is called ''thermal fixing,'' and experiments with macroscopic Gaussian intensity patterns reveal the following:

(i) At enhanced temperatures ($T\approx160$ °C) mobile protons compensate in $LiNbO_3$ the electronic space-charge fields, if the crystal contains a proton concentration which is at least

comparable with the concentration of filled electron traps.

(ii) Thermal fixing without protons is also possible; another charge compensation mechanism arises. It is expected that thermal fixing without protons enlarges the lifetime of the stored patterns.

(iii) There are no appreciable changes of the spontaneous polarization resulting from the fixing procedure.

(iv) The refractive-index patterns are developed by homogeneous illumination. Spatially modulated currents arise because of spatially modulated concentrations of filled and empty electron traps. Space-charge fields build up and modulate the refractive-index via the electro-optic effect; other contributions to the refractive-index changes are negligible.

(v) In $LiNbO_3$ crystals with large concentrations of Fe or Cu the space-charge fields can become so large, that breakdown occurs; only relatively small refractive-index changes can be obtained.

ACKNOWLEDGMENTS

Financial support of the Volkswagen-Stiftung (project ''Volumenphasenhologramme zum Vereinigen und Trennen der Lichtstrahlen von Diodenlasern'') and of the Deutsche Forschungsgemeinschaft (Sonderforschungsbereich 225) is gratefully acknowledged. One of us thanks the Volkswagen-Stiftung for a Ph.D. grant (Stipendienprogramm).

*FAX: +49/541/969-2670. Electronic address: kbuse@physik.uni-osnabrueck.de

[1] V. W. S. Chan, Sci. Am. **1995** (9), 56.
[2] D. Psaltis and F. Mok, Sci. Am. **1995** (11), 52.
[3] V. Leyva, G. A. Rakuljic, and B. O'Conner, Appl. Phys. Lett. **65**, 1079 (1994).
[4] A. M. Glass, D. von der Linde, and T. J. Negran, Appl. Phys. Lett. **25**, 233 (1974).
[5] E. Krätzig and R. Orlowski, Ferroelectrics **27**, 241 (1980).
[6] J. J. Amodei and D. L. Staebler, Appl. Phys. Lett. **18**, 540 (1971).
[7] J. J. Amodei, W. Phillips, and D. L. Staebler, Appl. Opt. **11**, 390 (1972).
[8] F. Micheron and G. Bismuth, Appl. Phys. Lett. **20**, 79 (1972).
[9] F. Micheron and G. Bismuth, Appl. Phys. Lett. **23**, 71 (1973).
[10] D. von der Linde, A. M. Glass, and K. F. Rodgers, Appl. Phys. Lett. **25**, 155 (1974).
[11] H. Vormann, E. Krätzig, Solid State Commun. **49**, 843 (1984).
[12] H. C. Külich, Opt. Commun. **64**, 407 (1987).
[13] R. A. Rupp, H. C. Külich, U. Schürk, and E. Krätzig, Ferroelectrics **8**, 25 (1987).
[14] K. Buse, L. Holtmann, and E. Krätzig, Opt. Commun. **85**, 183 (1991).
[15] K. Buse, F. Jermann, and E. Krätzig, Appl. Phys. A **58**, 191 (1994).
[16] D. L. Staebler, W. J. Burke, W. Phillips, and J. J. Amodei, Appl. Phys. Lett. **26**, 182 (1975).
[17] E. Krätzig, and R. Orlowski, Appl. Phys. **15**, 133 (1978).
[18] L. Arizmendi, J. Appl. Phys. **65**, 423 (1989).
[19] G. Montemezzani and P. Günter, J. Opt. Soc. Am. B **7**, 2323 (1990).
[20] G. Montemezzani, M. Zgonik, and P. Günter, J. Opt. Soc. Am. B **10**, 171 (1993).
[21] D. Kirillov and J. Feinberg, Opt. Lett. **16**, 1520 (1991).
[22] D. Zhang, Y. Zhang, C. Li, Y. Chen, and Y. Zhu, Appl. Opt. **34**, 5241 (1995).
[23] J. J. Amodei, W. Phillips, and D. L. Staebler, IEEE, J. Quantum Electron. **7**, 321 (1971).
[24] B. F. Williams, W. J. Burke, and D. L. Staebler, Appl. Phys. Lett. **28**, 224 (1976).
[25] V. I. Kovalevich, L. A. Shuvalov, and T. R. Volk, Phys. Status Solidi A **45**, 249 (1978).
[26] D. L. Staebler and J. J. Amodei, Ferroelectrics **3**, 107 (1972).
[27] G. Bergmann, Solid State Commun. **6**, 77 (1967).
[28] P. J. Jorgensen and R. W. Bartlett, J. Phys. Chem. Solids **30**, 2639 (1969).
[29] R. G. Smith, D. B. Fraser, R. T. Denton, and T. C. Rich, J. Appl. Phys. **39**, 4600 (1968).
[30] W. Bollmann, H.-J. Stöhr, Phys. Status Solidi A **39**, 477 (1977).
[31] S. Klauer, M. Wöhlecke, and S. Kapphan, Phys. Rev. B **45**, 2786 (1992).
[32] W. Meyer, P. Würfel, R. Munser, and G. Müller-Vogt, Phys. Status Solidi A **53**, 171 (1979).
[33] H. Vormann, G. Weber, S. Kapphan, and E. Krätzig, Solid State Commun. **40**, 543 (1981).
[34] R. Sommerfeldt, R. A. Rupp, H. Vormann, and E. Krätzig, Phys. Status Solidi A **99**, K15 (1987).
[35] J. M. Cabrera, J. Olivares, M. Carrascosa, J. Rams, R. Müller, and E. Diéguez, Adv. Phys. **45**, 349 (1996).
[36] V. V. Kulikov and S. I. Stepanov, Sov. Phys. Solid State **21**, 1849 (1979).
[37] P. Hertel, K. H. Ringhofer, and R. Sommerfeldt, Phys. Status Solidi A **104**, 855 (1987).
[38] R. Matull and R. A. Rupp, J. Phys. D **21**, 1556 (1988).
[39] M. Carrascosa and F. Agulló-López, J. Opt. Soc. Am. B **7**, 2317 (1990).
[40] L. Arizmendi, P. D. Townsend, M. Carrascosa, J. Baquedano, and J. M. Cabrera, J. Phys. Condens. Matter **3**, 5399 (1991).
[41] S. Kapphan and A. Breitkopf, Phys. Status Solidi A **133**, 159 (1992).
[42] H. Kurz, E. Krätzig, W. Keune, H. Engelmann, U. Gonser, B. Dischler, and A. Räuber, Appl. Phys. **12**, 355 (1977).
[43] J. L. Jackel, C. E. Rice, and J. J. Veselka, Appl. Phys. Lett. **41**, 607 (1982).
[44] R. Richter, T. Bremer, P. Hertel, and E. Krätzig, Phys. Status Solidi A **114**, 765 (1989).
[45] N. V. Kukhtarev, Sov. Tech. Phys. Lett. **2**, 438 (1976).
[46] R. Sommerfeldt, L. Holtmann, E. Krätzig, and B. C. Grabmaier, Ferroelectrics **92**, 219 (1989).
[47] R. Sommerfeldt, L. Holtmann, E. Krätzig, and B. C. Grabmaier, Phys. Status Solidi A **106**, 89 (1988).
[48] G. J. Edwards and M. Lawrence, Opt. Quantum Electron. **16**, 373 (1984).
[49] K. Onuki, N. Uchida, and T. Saku, J. Opt. Soc. Am. **62**, 1030 (1972).
[50] S. Fries and S. Bauschulte, Phys. Status Solidi A **125**, 369 (1991).
[51] R. T. Smith and F. S. Welsh, J. Appl. Phys. **42**, 2219 (1971).
[52] A. Mansingh and A. Dhar, J. Phys. D **18**, 2059 (1985).
[53] R. Sommerfeldt and E. Krätzig, SPIE **1126**, 25 (1989).
[54] S. H. Wemple, M. DiDomenico, Jr., and I. Camlibel, Appl. Phys. Lett. **12**, 209 (1968).